



Toward waste valorization by converting bioethanol production residues into nanoparticles and nanocomposite films

Guillaume N. Rivière^a, Florian Pion^b, Muhammad Farooq^a, Mika H. Sipponen^{a,c}, Hanna Koivula^d, Thangavelu Jayabalan^e, Pascal Pandard^e, Guy Marlair^e, Xun Liao^{f,g}, Stéphanie Baumberger^{b,*}, Monika Österberg^{a,*}

^a Department of Bioproducts and Biosystems, Aalto University, P.O. Box 16300, FI-00076, Aalto, Finland

^b Institut Jean-Pierre Bourgin, INRAE, AgroParisTech, Université Paris-Saclay, 78000, Versailles, France

^c Department of Materials and Environmental Chemistry, Stockholm University, Stockholm universitet, SE-106 91 Stockholm, Sweden

^d Department of Food and Nutrition, University of Helsinki, P.O. Box 66, 00014, University of Helsinki, Finland

^e Ineris, Parc Technologique ALATA, BP 2, 60550 Verneuil en Halatte, France

^f Quantis, EPFL Innovation Park Bât. D, 1015 Lausanne, Switzerland

^g Industrial Process and Energy Systems Engineering, Ecole Polytechnique Fédérale de Lausanne, EPFL Valais Wallis, Rue de l'Industrie 17, 1951 Sion, Switzerland



ARTICLE INFO

Article history:

Received 15 September 2020

Received in revised form 24 January 2021

Accepted 6 March 2021

Keywords:

Lignin nanoparticles

Biorefinery

Ecotoxicity

Cellulose nanofibrils

Lignocellulosic nanofibrils

Life cycle assessment

ABSTRACT

A “waste-valorization” approach was developed to transform recalcitrant hydrolysis lignin (HL) from second-generation bioethanol production into multifunctional bio-based products. The hydrolysis lignin (HL) was extracted with aqueous acetone, yielding two fractions enriched in lignin and cellulose, respectively. The soluble hydrolysis lignin (SHL) was converted into anionic and cationic colloidal lignin particles (CLPs and c-CLPs). The insoluble cellulose-rich fraction was transformed into lignocellulosic nanofibrils that were further combined with CLPs or c-CLPs to obtain nanocomposite films with tailored mechanical properties, oxygen permeability and antioxidant properties. To enable prospective applications of lignin in nanocomposite films and beyond, CLPs and c-CLPs were also produced from a soda lignin (SL) and the influence of the lignin type on the particle size and ecotoxicity was evaluated. Finally, the carbon footprint of the entire process from hydrolysis lignin to films was assessed and an integration to industrial scale was considered to reduce the energy consumption. While most previous work utilizes purified lignin and pristine and often purified cellulose fibers to produce nanomaterials, this work provides a proof of concept for utilizing the recalcitrant lignin-rich side stream of the bioethanol process as raw material for functional nanomaterials and renewable composites.

© 2021 The Authors. Published by Elsevier B.V. This is an open access article under the CC BY license (<http://creativecommons.org/licenses/by/4.0/>).

1. Introduction

Expansive utilization of fossil-based resources for fuels and packaging has a detrimental impact on land and marine ecosystems [1–4] and contributes to the acceleration of global warming [5,6]. In addition to biofuels, biomass-based materials are needed to advance adaptation of circular bioeconomy policies in Europe [7]. It is thus urgent to find sustainable resources to produce biodegradable and recyclable materials with a low carbon footprint [8–10]. Several bioethanol production processes using lignocellulosic biomass as a feedstock have been developed in the past few years [11]. These processes are mostly based on acid-catalyzed steam explosion and enzymatic hydrolysis, and generate a recalcitrant solid residue termed “hydrolysis lignin” that contains unhydrolyzed residual carbohydrates in addition to lignin phenolic

compounds and some minor components [12]. Though burning part of this by-product that represents more than 40% of the initial lignocellulosic feedstock is necessary to reduce fossil fuel consumption and ensure energetic autonomy of the process, its valorization into functional bioproducts would increase the overall sustainability of the process. One of the main obstacles to the valorization of this lignin-rich residue lies in its chemical heterogeneity, which hinders its direct applicability without further treatment or fractionation [13].

A few works have previously attempted to convert recalcitrant hydrolysis lignin into functional bio-based materials, but in these works only the lignin fraction was utilized to produce cationic lignin for water purification [14], or for antimicrobial and antioxidant CLPs while the non-soluble fraction was discarded [15]. Also, untreated lignocellulosic feedstocks from various biomass resources have been preferred in many prior studies [16–18]. The advantage of using native lignocellulose as raw material is that it generally contains less lignin than the hydrolysis lignin [13], which facilitates processing of cellulose into cellulose nanofibrils (CNFs) [16]. Although lignin is usually

* Corresponding authors.

E-mail addresses: stephanie.baumberger@inrae.fr (S. Baumberger), monika.osterberg@aalto.fi (M. Österberg).

removed by delignification and bleaching of CNF during the process, the presence of lignin may be advantageous in certain applications. This assumption has given rise to the production of lignin-containing CNFs, i.e., lignocellulose nanofibrils (LCNFs) from native feedstocks [17,18]. Actually, whereas CNFs provide high strength and stiffness to bio-based materials, e.g., for packaging applications [19,20], LCNFs can be used in coatings to bring further enhanced physico-chemical properties to cellulose-based materials, such as barriers against oil, water or oxygen [20–22]. The effect of residual lignin on the mechanical properties of films from cellulose fibrils has often been evaluated to determine if they would be suitable candidates to substitute bleached CNFs [17,18,23].

Native lignin in plant cell-walls and most lignin fractions recovered from lignocellulose biorefinery processes are poorly soluble in water. Their conversion into water-dispersible CLPs broadens their application range [24], in particular for uses where organic solvents are proscribed. Indeed, these spherical nanoparticles find numerous prospective applications in, e.g., drug delivery [25,26], adhesives [27], and sunscreens [28], and can be modified via chemical or enzymatic pathways [27,29], or via coating [25,30]. Notably, the naturally anionic CLPs can be rendered cationic via adsorption of water-soluble cationic lignin [30]. The applicability of the water-soluble cationic lignin and the c-CLPs has been demonstrated for water purification and more specifically, for removal of dyes [31] and viruses [32], and for stabilization of Pickering emulsions [30]. CLPs can also be easily integrated within multiple solid systems [24,33,34], and notably in CNF matrices [35–37]. The CLPs can be homogeneously spread onto a surface or evenly integrated within a composite material due to their dispersibility in water in comparison to non-colloidal crude lignins. Addition of CLPs allows tailoring of the antioxidant [35] or antimicrobial [38] properties of the resulting nanocomposite films. However, most of the previous reports combined CNF from fully bleached pulp and lignin particles prepared from separately isolated and purified lignin, both from different sources [35–37]. This approach is rather energy and chemical consuming and does not allow for use of the cellulose fibers for pulp or fuel. One recent paper reported the combination of cellulose and lignin from the same feedstock [16], but again, with native biomass that is not representative of the recalcitrant nature of the hydrolysis lignin from biorefinery processes.

The objective of this paper was to demonstrate the feasibility of valorizing hydrolysis lignin from a pilot-scale second generation (2G) bioethanol production process into various nanoscale materials demonstrating the utilization of the whole residual fraction with minimal waste production. A further objective was to assess whether conventional industrial solvents are suitable for dissolution and fractionation of the hydrolysis lignin. The solvent polarity shifting method was chosen to prepare CLPs from the soluble fraction of the hydrolysis lignin and, for comparison, from a highly pure soda lignin (SL). This method has already been applied on a few types of lignin including kraft, soda and organosolv lignins [24,39]. The extension to a soluble hydrolysis lignin (SHL) that has a different molecular structure and composition increased our understanding of the structure – property relation and the self-assembly mechanism of lignin into colloidal particles. Cationization of lignin was also extended to non-kraft lignins. The role of functional groups with respect to reactivity and formation of the c-CLPs is discussed. To ensure safe integration of the particles within biomaterials for environmental or health applications, their ecotoxicity was evaluated regarding size, charge and lignin source. Finally, LCNFs were obtained from the acetone:water insoluble fraction and combined with the different lignin materials produced from the SHL to make nanocomposite films. The mechanical resistance of these films as well as their antioxidant activity and oxygen barrier properties were evaluated, as they are the primary characteristics required for food packaging [40]. Finally, a life cycle assessment was performed to evaluate the energy consumption from a climate change point of view and to identify hot spots for future scale-up.

2. Results and discussion

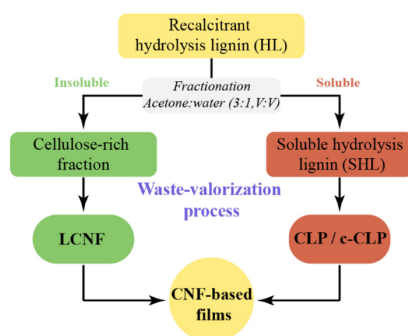
Our approach is based on the fractionation of a recalcitrant hydrolysis lignin from the bioethanol production process by selective extraction in an acetone:water solvent mixture (Scheme 1). This fractionation process was designed to recover a lignin-depleted cellulosic fraction (termed “cellulose-rich fraction”) used for preparation of LCNFs and a lignin-rich fraction (termed “soluble hydrolysis lignin” (SHL)) used to prepare CLPs, cationic lignin and c-CLPs. This section reports on the fractionation process and the characteristics of CLPs recovered from the hydrolysis lignin (HL) and the soda lignin (SL) used for comparison, then it focuses on the preparation of the nanocomposite films by assembling the HL fractions into a CNF-based nanocomposite.

2.1. Composition and solubility of HL compared to SL

In order to discuss the influence of lignin type on the CLPs characteristics, the detailed chemical composition of HL and SL was established and compared (Fig. 1a and Table S1). The two samples originated from grass feedstocks, wheat straw for HL and a mix of wheat straw and sarkanda bagasse for SL. SL was rich in lignin (89.1 wt% according to the Klason method) and contained only 1.85 wt% of carbohydrates, consisting of hemicelluloses mainly composed of arabinose and xylose. In contrast, HL contained 54.9 wt% of lignin and almost 39 wt% of carbohydrates, including 33.9 wt% of cellulose and 4.8 wt% of hemicelluloses mainly composed of glucose and xylose. Besides composition, a major difference between the two samples lay in the lower solubility of HL in most organic solvents and in aqueous media (Fig. 1b and Table S2). Indeed, whereas SL solubility ranged between 15 and 100%, it did not exceed 32% for HL. This could be in part explained by the presence of cellulose in this sample. The solubility data were used for the selection of the fractionation solvent, taking into account specifications relative to the selected CLP preparation method.

2.2. HL fractionation and CLPs recovery process

Out of the different methods to prepare CLPs [24], the nanoprecipitation method (also called solvent polarity shifting method) [25,32,35,41] was preferred here since it enables production of spherical particles with diameter below 200 nm. In this method, solubilized lignin, either in aqueous tetrahydrofuran (THF) or aqueous acetone, is quickly poured into water under rapid stirring. The organic solvent is removed by dialysis [32] or by evaporation [42] to yield a colloidal stable aqueous dispersion



Scheme 1. Concept for the valorization of 2G bioethanol recalcitrant residue by fractionation and re-assembly into CNF-based nanocomposite films.

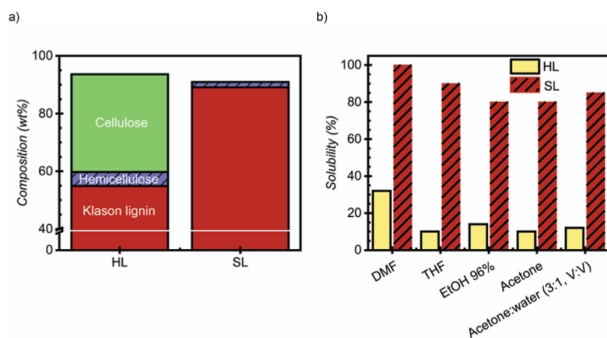


Fig. 1. a) Composition of hydrolysis lignin (HL) and soda lignin (SL) and b) their solubility in different organic solvents.

of spherical particles. The particles are easily modified, e.g., by adsorption of cationic polyelectrolytes [25,30]. This process was applied herein for the first time to recalcitrant hydrolysis lignin, in parallel to a reference soda lignin.

The choice of the fractionation solvent was driven by its suitability regarding the CLP production process and by the solubility of HL. SL solubility (Fig. 1b and Table S2) was not used as criteria, since it was highly soluble in the solvents commonly used for CLP preparation (90% for THF and 80% for acetone). The highest solubility (32%) of HL was obtained with dimethylformamide (DMF). However, the solvent must be easy to remove from the CLP dispersion by evaporation, which is not the case for DMF, unlike THF and acetone that have been found suitable for the production of CLPs from kraft lignin [35,41]. Due to its lower boiling point, acetone in a binary mixture with water was chosen as a good compromise, likewise to recent studies [25,32].

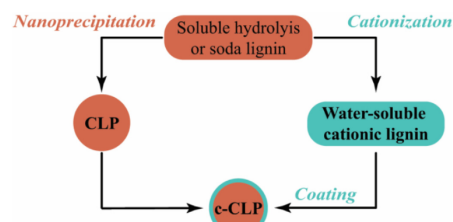
Using this process HL yielded 12 wt% of SHL fraction and 82 wt% of insoluble residue, giving a mass balance closure of 94%. As expected from the selective dissolution in organic solvents of phenolic compounds, with respect to carbohydrates, the lignin content was increased in the SHL fraction (82 wt%) and reduced in the insoluble fraction (44 wt%) compared to the initial HL lignin content (55 wt%). Taking into account the fractionation mass balance, these results indicate that 12% of the lignin contained in HL was extracted by the solvent. Due to its high lignin content, similar to that of SL, SHL was suitable for preparing different lignin-based materials. Herein, this fraction was used to prepare CLPs, water-soluble cationic lignin, and c-CLPs, as presented in Scheme 2. The last one was obtained by adsorption of water-soluble cationic lignin on the CLP surface [30]. On the other hand, the cellulose-rich

fraction was suitable for the production of LCNFs. Re-assembly of CLPs, cationic lignin or c-CLPs with LCNFs allowed for the preparation of nanocomposite films (Scheme 2).

2.3. Effect of lignin structure on the formation of colloidal particles

In order to assess the influence of lignin structure on lignin colloidal properties, CLPs were prepared from the SHL fraction and from SL using the technique discussed above. Indeed, the samples showed similar lignin content (less than 10% difference) but differed in their structure, in particular in terms of molecular weight (Fig. 2a and Fig. S1). The SHL weight average molecular weight was 27% higher than that of SL (3510 and 2570 g mol⁻¹ respectively). Furthermore, both lignin fractions displayed different chemical compositions as showed in Table S2. SHL contained a higher amount of aliphatic hydroxyls and a lower amount of phenolic hydroxyls. However, they had similar amount carboxylic acids. Both, molecular weight and functional groups are known to influence the particle size [43].

No differences in term of charge were observed between the lignins for the uncoated CLPs (Fig. 2b). Both fractions had a high enough anionic charge to ensure good colloidal stability. For electrostatic stabilization high enough anionic or cationic charge is needed. In contrast, a clear difference in CLP size was observed (Fig. 2c), with a higher diameter for SL (97 against 68 nm for the SHL fraction at pH 5). This difference in particle size is likely related to the higher molecular weight of SHL. Indeed, a similar decrease of CLP diameter was previously observed both upon lignin polymerization by laccase [27], and upon fractionation [44]. The same trend was observed when using a mixture of THF:water (3:1, w; w) for lignin dissolution (CLP diameter of 138 and 110 nm for the SL and SHL fraction, respectively; Fig. S2). These results showed that CLPs with larger diameter are formed from THF:water precipitation compared to acetone:water precipitation system, confirming previous observations [24]. A higher molecular weight is associated with lower water-solubility, leading to more rapid nanoprecipitation and we speculate that this will lead to the formation of smaller particles. The chemical structure is also considered as a determining factor for the particle size such as the ratio between S/G ratio or high content in phenolic hydroxyls and carboxylic acids or the type of linkages within the structure [43]. SHL contained more aliphatic hydroxyls increasing the hydrophobicity of the lignin, yielding to smaller particles, while SL had a higher hydrophilicity due to a higher amount of phenolic hydroxyls. However, more research is needed to fully understand the particle formation mechanism.



Scheme 2. Pathways for lignin transformation into cationic colloidal lignin particles.

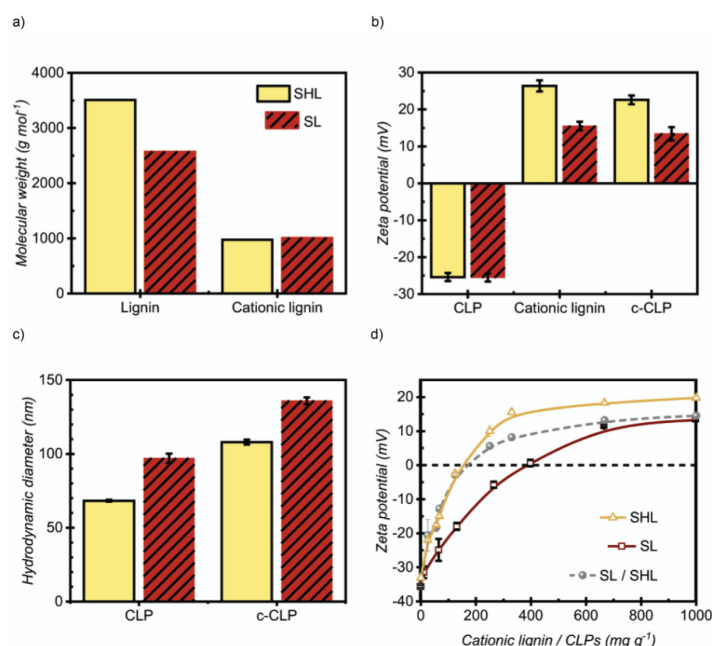


Fig. 2. Characterization of lignin fractions either made from SHL or SL. a) Weight average molecular weight (Mw) of the acetone:water soluble fractions and their cationized counterparts. b) Zeta potential of CLPs, cationic lignins and c-CLPs at pH 5. c) Hydrodynamic diameter of CLPs and c-CLPs at pH 5. d) Evolution of Zeta potential via adsorption of cationic lignin on anionic CLP surface.

Cationic CLPs were prepared to demonstrate the effect of lignin composition on the functionalization of CLPs. Cationic lignin was first produced in aqueous alkaline solution via epoxide ring-opening grafting to the aliphatic and phenolic hydroxyl groups of lignin with glycidyltrimethylammonium chloride (GTMAC). The resulting water-soluble lignin bearing quaternary ammonium ions is described here simply as cationic lignin. This cationic lignin was then used to prepare c-CLPs by coating anionic CLPs as previously demonstrated for kraft lignin [30,31]. A similar cationization procedure was applied to SL and SHL, except that the amount of GTMAC was increased by a factor of 2 for both lignins to ensure complete reaction and to reduce the formation of insoluble products. A small fraction of insoluble cationic lignin is formed during the cationization reaction. Unfortunately, Sipponen et al. [30] have shown that this insoluble product cannot be transformed into spherical CLPs. The adapted procedure led to a yield above 75% of soluble cationic product in comparison to the 50% previously observed with kraft lignin [30]. The Zeta potential of the formed cationic lignins are shown in Fig. 2b (+15.5 mV for SL and +26.4 mV for SHL against +21.7 mV for the kraft lignin [32] at pH 5) and indicates the lower reactivity of the SL compared to the kraft lignin. In contrast to cationized SL, the cationic SHL showed a high positive net charge, which is beneficial for the stability of the c-CLPs. Additionally, as shown in Fig. 2a, the cationization reaction induced a reduction of the apparent molecular weight of both lignin fractions that approached similar values (1008 g mol⁻¹ for SL and 975 g mol⁻¹ for SHL). This reduction could be due to the lower solubility of higher molecular weight cationized lignins, but it does not explain the observed difference in reactivity. Since

cationization takes place through the substitution of phenolic and aliphatic hydroxyl groups [30], these results were assessed by comparing changes in the concentrations of the hydroxyl functional groups.

Table S1 shows that SL contains the highest total aliphatic and phenolic content (6.64 mmol g⁻¹ against 5.6 mmol g⁻¹ and 5.94 mmol g⁻¹ for the SHL fraction and the kraft lignin, respectively). These data suggest that the amount of GTMAC is still not high enough to get a sufficient substitution rate of SL. Besides the availability of functional groups for substitution, the presence of ionizable non-substituted groups likely to carry anionic charges has to be taken into account. Indeed, these anionic charges counteract the effect of cationization and lead to a lower Zeta potential of the cationized lignin. Accordingly, the content of carboxylic acids was higher in SL (0.86 mmol g⁻¹) in comparison to the kraft lignin (0.57 mmol g⁻¹). It means that there is an important source of anionic charges that cannot be substituted during the cationization in SL and in SHL. Therefore, the high content of carboxylic acids and hydroxyls is responsible for the low cationic charge of the soda lignin. The similar content of carboxylic acids of SHL and SL encouraged us to directly use the adapted procedure for the cationization of SHL. The impact of the charge of the cationic lignin as well as the size of the CLPs on the formation of the c-CLPs was then evaluated.

Fig. 2d shows the result of progressively coating particles by gradual addition of cationic lignin to a CLP dispersion. Compared to the relatively low amount of cationic lignin (40 mg g⁻¹) required to render kraft lignin CLPs cationic by adsorption [30], the minimum amount of cationic lignin required to cationize 1 g of anionic CLPs was 10 times higher for SHL and 17 times higher for SL. The two main parameters

to be considered to explain this large difference are the particle size and the available functional groups on the CLP surface. Indeed, for a given mass of lignin in the colloidal system, the total surface of particles to be covered decreases when the particle size increases, and at constant particle size, a higher content of anionic groups leads to a higher consumption of cationic lignin for particle cationization. As expected, more cationic lignin was needed to cationize the <100 nm sized CLPs in the present study, as compared to previous results for CLPs from the kraft lignin of about 274 nm [30], confirming the effect of particle size. The particle size difference between the SHL fraction and the soda lignin, 68 and 97 nm respectively, seems, however, to be too small to observe an impact on c-CLP formation. Instead, the availability of reacting functional groups was expected to be more important for the observed differences between these two lignins. Accordingly, the higher amount of cationic lignin required to cationize SL CLPs was consistent with its higher content of anionic groups. To further elucidate this phenomenon, a third experiment was performed by coating SHL CLPs by cationic SL. As shown in Fig. 2d, the curve followed the trend of the SHL CLPs in the anionic range and switched to the trend of the cationic SL in the cationic range. This observation confirmed that the lower content in carboxylic acids and phenolic hydroxyls in SHL accounted for its more efficient cationization compared to SL. Once all the negative charges are compensated, the cationicity of the c-CLPs is governed by the charge of the cationic SL in the coating.

For further specific tests or applications (such as integration within films or for ecotoxicity), the ratio of water-soluble cationic lignin on CLPs was fixed at 400 mg g⁻¹ for SHL and at 1000 mg g⁻¹ for SL to obtain stable dispersions of clearly cationic CLPs. The Zeta potential and the size of the particles obtained using these ratios are shown in Fig. 2b and c, respectively.

2.4. Ecotoxicity of lignin nanoparticles

Very little is known about the leaching of lignin or of CLPs from engineered materials and what impact especially nanoscaled lignins have on the environment, and on aquatic and terrestrial animals. Despite the fact that they have been described as non-toxic in low concentrations [24], utilization of nanoparticles for healthcare or food applications remains controversial due to unknown health risks. In general, the term nanoparticle (NP) refers to particles with a diameter below 100 nm, but it also commonly used for particles up to a diameter of 500 nm. From the safety perspective, a common hazard to consider for sustainable use of finely divided biomass residue, like lignin, is dust inhalation [45] and dust explosion hazards [46,47], the latter becoming more severe as the particle size decreases to the nanoscale [48]. Given the fact that in the studied value chain lignin nanoparticles are essentially processed in the form of aqueous colloids, these risks are eliminated.

Various aqueous lignin dispersions have also been studied for water purification (for removal of dyes [31,49], heavy metals ions [50,51], or to agglomerate viruses [32]), but the ecotoxicity of spherical CLPs has not yet been evaluated. The biocompatibility of CLPs [26,52] for drug delivery systems has already been studied and the viability of yeasts and microalgae was not affected after a short duration of exposure to lignin nanoparticles [53]. We extended this frontier by studying the effect of

CLPs and c-CLPs on freshwater aquatic organisms *Daphnia magna* (a small planktonic crustacean) and *Pseudokirchneriella subcapitata* (a microalga). Table 1 shows the toxicity against a) *D. magna* expressed as EC50 48 h (i.e., the concentration that causes 50% reduction in living population within 48 h), and b) against *P. subcapitata* as EC10 and EC50 (i.e., the concentrations of lignin that cause respectively 10% and 50% of algal growth inhibition after 72 h). No inhibitory effects were observed on the mobility of *D. magna* up to 500 mg L⁻¹ of CLPs (the highest tested concentration). In contrast, the algal growth inhibition test determine the EC50 values for the four tested lignin materials.

The EC 50 ranged from 15.9 mg L⁻¹ for SL CLPs to 34.2 mg L⁻¹ for the SHL c-CLPs, showing a higher toxicity than conventional alkali lignin towards the marine algae *Phaeodactylum tricornutum* [54]. In our case, the possible internalization of CLPs can result in elevated local intracellular concentrations and thus showed lower EC50 values. It seems that SL is slightly more inhibitory than SHL regardless of the charge of the particles. To overcome the limitations and interference from solid particles observed in previous studies [55,56], the algal growth inhibition test was designed to maximize contact between the living organisms and the CLPs. Moreover, two measurement methods were used to determine the algal biomass (cell count: Table 1 and in vivo fluorescence: Table S3). The in vivo fluorescence method led to similarly ranged results but the difference between SL and SHL was less pronounced than with the cell count method. Thus, the four lignin materials can be considered to have a similar toxicity range.

For accurate comparison, particles with similar sizes must be considered. Indeed, it has been demonstrated that smaller particles are more toxic than larger ones [57]. It is also relevant to select particles that can be used for similar applications to consider CLPs as potential substitutes. For this reason, a comparison to earlier work with nanoparticles (NPs) of CuO, ZnO and TiO₂ was made. Lignin and CLPs have been notably studied for antimicrobial applications [15] similarly to TiO₂ [58]. CuO have been notably studied for the removal of arsenic and organic pollutants [59], or deactivation of viruses in water [60], while lignin has been studied for removal of dyes [31,49], heavy metal ions [50,51], or viruses [32]. Finally, ZnO is used as UV-blocker [58], as have lignin particles [61,62].

The toxicity of CuO, ZnO and TiO₂ NPs has been evaluated against the same species (*D. magna* and *P. subcapitata*) [63,64]. These inorganic NPs showed higher toxicity than our lignin particles against both species. For instance, the EC 50 (72 h) was about 0.042, 0.71 and 5.83 mg L⁻¹ for ZnO, CuO and TiO₂ NPs respectively against *P. subcapitata* [64]. Thus, CLPs and c-CLPs could be considered as potential candidates for substituting or reducing the utilization of inorganic NPs in their respective applications due to their similar properties. Finally, given their relatively low ecotoxicity against the two aquatic organisms studied here, their integration within packaging materials is encouraged. One of the promising approaches it to entrap CLPs in polymeric matrices such as LCNFs that can also be considered safe from an environmental point of view.

2.5. Nanocomposite films with antioxidant activity and oxygen barrier properties

Bio-based films and membranes are promising materials for barrier materials in packaging applications [40]. These films can act as

Table 1
Evaluation of toxicity of CLPs and c-CLPs against *Daphnia magna* and *Pseudokirchneriella subcapitata* (also known as *Raphidocelis subcapitata*) via the cell count method.

Lignins	OECD 202 <i>Daphnia magna</i>		OECD 201 <i>Pseudokirchneriella subcapitata</i>			
	EC 50 24 h (mg L ⁻¹)	EC 50 48 h (mg L ⁻¹)	EC 10 72 h (mg L ⁻¹)	95% confidence interval	EC 50 72 h (mg L ⁻¹)	95% confidence interval
SL CLPs	>500 ^a	>500 ^a	3.5	2.7–4.5	15.9	14.3–17.6
SL c-CLPs	>500 ^a	>500 ^a	6.2	5.4–7.0	18.3	17.4–19.2
SHL CLPs	>500 ^a	>500 ^a	9.4	6.5–12.9	30.9	27.1–35.3
SHL c-CLPs	>500 ^a	>500 ^a	9.5	5.3–14.6	34.2	27.4–45.3

^a Higher than the concentration tested.

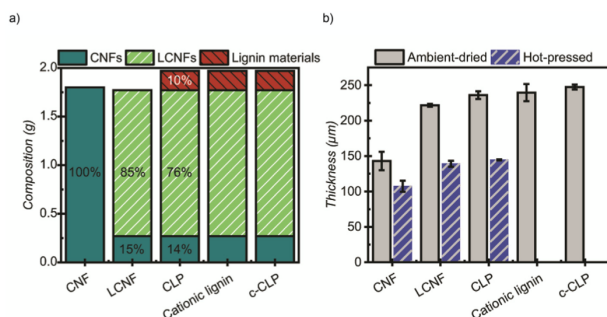


Fig. 3. a) Composition (based on dry content during film preparation) of CNF and composite films prepared from HL fractions. b) Thickness of ambient-dried and hot-pressed films (HP).

barrier against water, grease, oil, or air [20,21], although to obtain a good water vapor barrier further chemical modification of the biobased films is needed [65]. Chemical functionalities such as antimicrobial, antioxidant and anti-UV have also been conferred to biobased films [19,40,66]. Finally, mechanical resistance and flexibility are essential for good technical performance. Here, we measured the mechanical resistance and the oxygen permeability, and evaluated the antioxidant activities of the nanocomposite films produced from LCNFs and other lignin materials based on the two fractions recovered from the hydrolysis lignin.

Films with the following five different compositions were prepared (Fig. 3a); a pure CNF film for reference (named CNF); a film containing LCNFs and 15 wt% of pure CNFs (named LCNF); and films containing LCNFs and CNFs with 10 wt% of CLPs, c-CLPs or water-soluble cationic lignin (named CLP, c-CLP and Cationic lignin respectively). First, wet films were prepared by pressure-assisted filtration [35]. The obtained films were then dried between blotting papers either over a week under a 5 kg load at 23 °C and 50% relative humidity (RH) or hot-pressed at 100 °C (Fig. 3b). The ambient-dried films with blotting papers are simply called "films", e.g. "CNF film", while the hot-pressed films are called "(HP) films", e.g. "CNF (HP) film".

As expected, hot-pressing reduced the thickness of the films (Fig. 3b). Since the LCNFs already contained a significant amount of lignin (37.2%), the difference in lignin content of the films was relatively low. The additional lignin in the form of CLPs, c-CLPs or cationic lignin (Table S1) increased the lignin amount only by 4.6 wt%. Since the ambient-dried films were too fragile to be handled, the tensile tests were performed only on CNF (HP), LCNF (HP) and CLP (HP) (Fig. 4), and stress and strain values were subsequently determined (Table S4). The presence of lignin reduced the strength of the films, as expected from previous studies [17,20,21,35]. The nanocomposite films prepared from pure CNF in this study exhibited a tensile strength of 118.7 ± 8.0 MPa and tensile strain of $2.4 \pm 0.4\%$. In comparison, the films prepared from LCNF showed a decline in the tensile strength (31.4 ± 4.7) and strain (0.8 ± 0.15). Similarly, the tensile young's modulus also displayed a decrease from 8.5 ± 0.3 GPa for pure CNF to 4.5 ± 0.4 GPa for LCNF and 4.3 ± 0.3 GPa for CLP films.

The combination of pure CNF and CLPs have been found to yield nanocomposite films with increased strength compared to CNF alone, but the maximum strength was observed at 10 wt% CLP and increasing the lignin content to 20% decreased the strength, in line with our observations [35]. In that study, it was also observed that the use of c-CLPs instead of CLPs did not significantly change the mechanical properties, hence the effect of cationization on the mechanical properties was not studied here.

Chen et al. [18] evaluated the effect of residual lignin from poplar wood on the mechanical properties of the LCNF films and obtained a stress at break of 22.6 MPa at a lignin content of 22.1%. Despite the fact that residual lignin was present in the interconnected LCNF network, this value is lower compared to the 31.4 MPa that was obtained here with LCNF (HP) film. A few studies have also reported higher mechanical strength of films prepared from LCNF [23,67]. However, what is typical for these studies is that they used LCNF prepared from native cellulose fibers and the lignin content never exceeded 15 wt%.

The mechanical properties of the composite films described in the present study remained suitable for packaging applications, even with the lower strain-at-break of the LCNFs (Fig. 4), and despite the fact that only c.a. 15 wt% of pure CNF was used to reinforce the material and that the lignin content was as high as 37–41 wt%. The presence of hemicelluloses (5 wt%) associated to cellulose and lignin in the recalcitrant hydrolysis lignin might contribute to the cohesion of the material. [68,69] In view of this result, the films were further assessed for their oxygen barrier properties and antioxidant activity.

The oxygen permeability (OP) of the nanocomposite films was evaluated at 50 and 80% RH. At 50% RH, only the films dried under a 5 kg load over a week in a 50% RH room were tested (Fig. 5a), while all the films (except the cationic ones) were tested at 80% RH (Fig. 5b). The

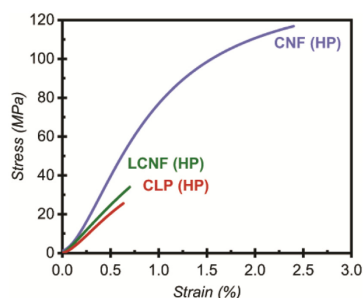


Fig. 4. Tensile stress-strain curves of hot-pressed (HP) films. Representative stress-strain curves, with the lowest difference in tensile stress and strain-at-break values with respect to the mean values are shown. CNF (HP) was made of pure CNFs, LCNF (HP) contained 15% of CNF (15 wt%) and 85% of LCNFs, and CLP (HP) contained 14% of CNFs, 76% of LCNFs and 10% of CLPs (dry matter based).

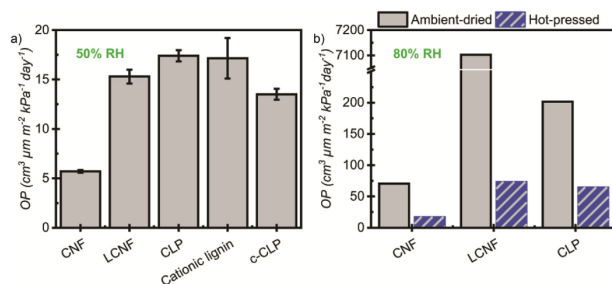


Fig. 5. Oxygen permeability (OP) of the films dried at room temperature with low load and hot-pressed films at a) 50% and b) 80% relative humidity.

reference CNF films displayed similar oxygen permeability as previously published results [70]. Minor differences in oxygen permeability were observed at 50% RH between all the films that contained LCNFs. The addition of CLPs and cationic lignin in the films slightly increased the permeability, while the addition of c-CLPs slightly reduce it. It is also interesting that films containing soluble cationic lignin displayed larger error bars, indicating a more heterogeneous material compared to the films containing spherical particles. However, all films were less efficient oxygen barriers than pure CNF films. Disruption of intra-fibril hydrogen bonding caused by the inclusion of lignin clusters from the LCNFs (as showed in AFM images in Fig. S3) is anticipated to decrease the OP of the nanocomposite films. Furthermore, the HP nanocomposite films demonstrate better OP values compared to ambient dried film clearly indicating the densification of the film structure upon hot-pressing. The density of the pure CNF film dried at ambient conditions is $879 \pm 65 \text{ kg m}^{-3}$, whereas the hot-pressed film revealed slightly higher density value of $1031 \pm 110 \text{ kg m}^{-3}$. For lignin containing films the drying process had insignificant effect on the density values as tabulated in Table S5. Additionally, the mass balance of the dried films suggests that the same amount of materials was integrated within the LCNFs whatever its charge or shape. This low difference in OP values may be due to the low contribution of lignin addition to the total weight of the films (only 10 wt%).

The oxygen permeability was also tested at 80% RH to determine the limitations of the LCNFs. Both ambient-dried and HP films were tested. All the films showed higher permeability at this higher relative humidity, which reflected lower hydrogen bonding between fibrils due to the presence of adsorbed water molecules in the materials. The value of 7100 for the ambient-dried LCNF film indicates that there would have been significant leakage in the films containing LCNFs made from residues. However, all the HP films exhibited lower oxygen permeabilities than the ambient-dried ones. A fourfold decrease in oxygen permeability was observed for the reference CNF film, which could be explained by increased interactions between the fibrils (hydrogen bonds and van der Waals interactions) due to pressing. A reduction to 1/3 of the value of ambient-dried films was observed for the hot-pressed CLP films. This reduction could be explained by partial impregnation of the fibrils by lignin at high-temperature under pressing, [22,35] even if the temperature of the press was not high enough to melt the lignin.

Rojo et al. reported similar permeability for lignocellulosic films at 50% RH, but a 2 times lower permeability at 80% RH compared to the LCNF (HP) film [23]. This difference is likely due to a lower lignin content in their films with favorable distribution on the fibril surface. In agreement with our observations, Rojo et al. also reported about a four-fold increase in oxygen permeability for films containing lignin compared to pure CNF films.

The films CLP (HP) and LCNF (HP) showed more promising oxygen barrier properties at high humidity despite the high lignin content and low amount of pure CNFs than many previously reported materials using LCNF, and comparable oxygen permeability to plastics, such as poly(ethylene terephthalate) (PET) or poly(lactic acid) at 50% RH [71]. Additionally, the present films showed lower oxygen transmission rates (OTR) compared to LCNF-coated paper [20]. The highest values were about $7.50 \text{ cm}^3 \text{ m}^{-2} \text{ day}^{-1}$ at 50% RH and $136 \text{ cm}^3 \text{ m}^{-2} \text{ day}^{-1}$ at 80% RH, both obtained with CLP films. (Detailed OTR values are presented in Table S5). Thus, it seems that the recalcitrant residues from the bioethanol production could find utilization as active coatings in the packaging industry or as breathable materials. For this reason, the antioxidant properties of the films were tested.

Lignin is well-known to have antioxidant properties due to the presence of phenolic groups [72–76]; this functionality has been frequently harnessed in composite films and composite materials [35,66]. The antioxidant activity of the films was evaluated using the radical cation of 2,2'-azino-bis-(3-ethylbenzothiazoline-6-sulfonic acid) diammonium salt (ABTS^{•+}) (Fig. 6). Due to the higher thickness and higher lignin content of the films compared to our previous work [35], a kinetic study (Fig. S4) was carried out with circular pieces of CLP films. The absorbance reduction appeared to reach a plateau after 1 h of mixing in the ABTS^{•+} solution. Thus, the size of the specimens was reduced to keep a mixing time of 1 h in order to have enough time for the ABTS^{•+} to penetrate the films and get more reliable results. Furthermore, the interactions occurred at the liquid/solid interface [35].

The results of the antioxidant tests (Fig. 6) were consistent with previous results [35]. Indeed, the ambient-dried CNF films did not show any antioxidant activity (AA), unlike the lignin-containing films. As observed with the oxygen permeability results, the charge of the added lignin did not affect the activity. In the context of AA, this result is more interesting since it suggests that adsorption of the radical cation on anionic CLPs or possible charge repulsion with c-CLPs did not interfere with the result. Furthermore, utilization of a hot-press to dry the films had a positive impact on the antioxidant activity. Indeed, even the pure CNF films saw their AA slightly increased due to hot-pressing. This is probably due to a physical entrapment or absorption of the dye in the film matrix that became denser upon the hot-pressing. As expected, the antioxidant activity increased further when more lignin was added in the form of CLPs, cationic lignin or c-CLPs. Since the increase in lignin content was low, the observed increase in activity was also minor. However, the antioxidant activity was lower than previously reported [35]. In the previous study, films containing 10 wt% of lignin reached 1.21 mg of tannic acid equivalent (TAE) per gram of sample TAE, while films containing 50 wt% lignin reached 2.07 mg TAE g^{-1} [35]. This difference can be explained by the higher

G.N. Rivière, F. Pion, M. Farooq et al.

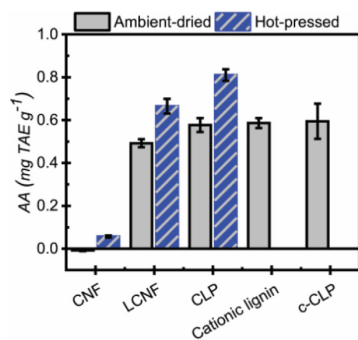


Fig. 6. Antioxidant activity (AA) of the films expressed in mg of tannic acid equivalent (TAE) per gram of sample.

phenolic hydroxyl groups content of the kraft lignin compared to HL (4.05 mmol g⁻¹ against 0.70 mmol g⁻¹). The difference in carboxylic group content (0.13 mmol g⁻¹ for the hydrolysis lignin against 0.57 mmol g⁻¹ for the kraft lignin) might also contribute to this difference [77].

These results warrant further investigations towards integration of 2G bioethanol residue within packaging products. The LCNFs and the CLPs could work as coatings, in multilayer barrier systems or as components in biocomposites to bring added antioxidant properties instead of as free-standing films. In the spirit of circular economy, the goal of finding valuable applications for residues should not be forgotten. Furthermore, the low toxicity of the lignin particle, combined with the potential of composite materials as active coatings, encouraged us to calculate the energy consumption of our process and to consider how it could be improved.

2.6. Carbon footprint from life cycle assessment and feasibility of scaling up

A life cycle assessment (LCA) was performed for the functional unit producing 1 kg of nanocomposite films containing CLPs to identify hotspots and opportunities of mitigating greenhouse gas (GHG) emissions measured by carbon dioxide-equivalent, also called the carbon footprint. Since cationic lignin or c-CLPs did not show significant improvements in term of either antioxidant or barrier properties the LCA study was focused on unmodified CLPs.

Fig. 7 shows the life cycle carbon footprint of three scenarios broken down by different inputs; i) a baseline scenario determined from the lab-scale experimental data with the European average grid mix and heat from natural gas, assuming 99% recovery of acetone [78]; ii) an optimized scenario by scaling-up to improve energy efficiency; iii) a further optimized scenario by considering low-carbon electricity and heat.

In the baseline scenario, 98.9% of the GHG impact is related to energy consumption, mainly comprising of the stirring in the fractionation step of separating the hydrolysis lignin into soluble lignin and lignocellulose powders, the evaporation of acetone in the CLP production, the filtration step for the LCNF production, and the mixing step for the preparation of the final composite film. Improving the energy efficiency of the process could, consequently, decrease the carbon footprint of the composite film production. Indeed, a reduction in the carbon footprint from the 179 kg CO₂-eq/kg film for the lab scale production to 26 kg CO₂-eq/kg film (85.4% of GHG reduction) in the scaled-up scenario could be achieved, as detailed in the section below. A further reduction to 3 kg CO₂-eq/kg film (98.4% of GHG reduction) can be achieved by switching energy sources in the scaled-up scenario to low-carbon waste energy or

Sustainable Materials and Technologies 28 (2021) e00269

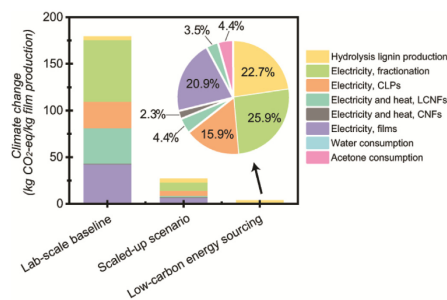


Fig. 7. Strategies of reducing the life cycle carbon footprint of the nanocomposite film production (kg CO₂-eq/kg film).

renewable energy. In the most optimized case, material production (including the hydrolysis lignin, the raw material for CNFs production and filtration glass fiber production) becomes important to consider, accounting for 22.7% of the life cycle GHG emissions. In comparison, production of lignin particles from biorefineries has been reported and showed a baseline scenario with a higher carbon footprint but mainly induced by solvent consumption [79]. It has also been demonstrated that the integration of bioethanol and biomass thermal energy in that process induced a complete reduction of the input energy.

For the scaled-up scenario, we considered the following adaptations from the baseline scenario: i) for the fractionation phase, the time required for stirring was reduced from 12 h to 2 h [80], or to 16.7% of the energy consumption in the baseline scenario; furthermore, the electricity used for centrifugation was based on a large Decanter centrifuge equipment with the electricity consumption of 6 m³/14 kWh [81]; ii) for the CLP production phase, the electricity use for evaporation of acetone was now based on a large scale Rotavapor® R-220 Pro equipment with the electricity consumption of distilling 27 l of acetone/6.3 kWh [82]; iii) for the production of LCNFs, the energy consumption values reported by Arvidsson et al. [83] was used, including 9.6 MJ of heat and 0.44 MJ of electricity/kg for the enzymatic pretreatment and 8 MJ of electricity/kg for the mechanical fibrillation; iv) we assumed that the energy use for mixing/stirring can be reduced to 16.7% of the energy consumption in the baseline scenario following the same assumption of the scaled-up stirring step as in the fractionation stage.

2.7. Further potentials of optimizing nanocomposite film production

Beyond the adaptations considered in the scaled-up scenario mentioned above, alternative methods can also be used for potentially optimizing the different steps of the process. For instance, roll-to-roll type of preparation of LCNFs can be considered [84] or melt-blending can be an alternative method to prepare composite materials from lignocellulosic powders [85]. Additionally, CLPs can be prepared with a continuous flow tubular reactor [86]. The improvement of the recycling rate for either acetone or ethanol can also potentially reduce the impact associated with solvent use. Although acetone is a solvent that can be easily recycled, it could be substituted by ethanol, which has a lower environmental impact [87]. The solubility of the hydrolysis lignin was slightly higher in ethanol compared to acetone, also (Table S2). Utilization of ethanol would also allow integration within an ethanol organosolv process [43]. Although ethanol seems suitable for the hydrolysis lignin due to similar solubility as acetone, some previous results suggested that the yield of CLP production was lower when aqueous ethanol was utilized

instead of aqueous THF at high concentration [88]. A high lignin concentration needs to be reached to reduce the energy consumption, but this concentration has to be suitable for formation of CLPs. Alternatively, a three-solvent system including ethanol, THF and water, can be used to enable higher lignin concentrations [78].

3. Conclusion

This study demonstrated the feasibility to valorize a recalcitrant residue of a 2G bioethanol production following a "waste-valorization" approach. After fractionation of the hydrolysis lignin using aqueous acetone as solvent, CLPs and c-CLPs were successfully prepared from the soluble fraction in the exact same way as with a soda lignin of high purity, while LCNFs were prepared from the insoluble fraction. The formation of cationic colloidal lignin particles was found to depend on the functional group distribution within the lignin and particularly on the balance between hydroxyl groups available for grafting and the residual ionizable groups as a source of anionic charge. Moreover, the size of CLPs appeared to have a lower influence on the formation of the corresponding c-CLPs within the size-range studied. Ecotoxicity of lignin particles was assessed with respect to both the charge and size of the particles, both CLPs and c-CLPs were found to exhibit lower toxicity than common metal oxide nanoparticles, encouraging further studies towards environmental and medical applications of the lignin particles. LCNFs produced from extracted hydrolysis lignin showed interesting physico-chemical properties with respect to packaging film applications, namely oxygen barrier and antioxidant activity and an adequate mechanical performance in combination with a low amount of pure CNF. These materials could find suitable applications in packaging coatings or composites. The life cycle carbon footprint analysis revealed the importance of considering the production scale difference, and using LCA to identify hotspots in the early technology development stage. It also demonstrated that the carbon footprint of producing functional nanomaterials or composite films can be significantly improved from the lab-scale by improving energy efficiencies through scale-up, solvent recycling rate and by sourcing low-carbon energy. Overall, these findings promote the use of hydrolysis lignin and make its valorization a realistic scenario for lignocellulosic biorefineries.

4. Experimental section

4.1. Materials

The hydrolysis lignin (HL) was produced from wheat straw via steam explosion pretreatment followed by enzymatic hydrolysis and was received as a wet cake (c.a. 50 wt% of water). Before utilization, the sample was dried under a fume hood for 4 days at room temperature and ambient pressure, then manually milled and dried under vacuum at room temperature to obtain a fine powder. For the sake of confidentiality regarding current industrial developments, the authors cannot mention the source of the hydrolysis lignin.

The soda lignin (SL) (Protobind 1000) was produced from a mixture of wheat straw and Sarkanda grass bagasse via a soda process and purchased from GreenValue Enterprises LLC (U.S.A.). It was received as a fine brown powder and used without any prior treatment.

Pure CNF was prepared as described previously [70]. Briefly, never dried bleached hardwood kraft pulp fibers were washed into sodium form following a procedure reported by Swering et al. [89] Fibrillation was performed by using a type M-110P microfluidizer (Microfluidics, Newton, Massachusetts, USA) in a single pass through a series of 400 and 200 μm chambers, followed by six passes through a series of 400 and 100 μm chambers. The operating pressure was 2000 bar. The resulting CNF suspension of 2 wt% was stored at 4 °C when not in use. The raw material and the fibrillation method were the same as previously used, so we expect to have an average width of 5–20 nm and length of several micrometers and Zeta-potential around -3 mV [90].

ABTS, HCl (33%), tannic acid, GTMAC and sodium persulfate were purchased from Sigma-Aldrich. Whatman® glass microfiber filters Grade GF/F were also purchased from Sigma-Aldrich. Dialysis membranes 6–8 kDa and 1 kDa were purchased from Fisher Scientific. All water used in this work was deionized water.

4.2. Compositional analysis of the lignin fractions

Klason lignin (KL) content was determined gravimetrically after a two-step sulfuric acid hydrolysis of the sample (300 mg), with correction for ash content, as described by Dence [91]. Neutral sugars were analyzed by a sequential three-step acidic hydrolysis of the sample (10 mg) first, aqueous trifluoroacetic acid (TFA, 2.3 M, 2 h, 110 °C), followed by two sulfuric acid steps (51% p/p H_2SO_4 , 1 h, ambient temperature, then 5% p/p H_2SO_4 , 2 h, 100 °C). The neutral monosaccharides recovered after TFA and H_2SO_4 hydrolysis were assigned to hemicellulose-derived sugars and cellulose-derived glucose, respectively, and determined by high-performance anion-exchange chromatography with amperometric detection with fucose as internal standard according to Sipponen et al. [92] Quantitative ^{31}P NMR and the related sample preparation, including derivatization with 2-chloro-4,4',5,5'-tetramethyl-1,3,2-dioxaphospholane (TMDP, Sigma-Aldrich, France), were performed according to a reported procedure [93]. Lignin samples (20 mg) were dissolved in 400 μL of a mixture of anhydrous pyridine and deuterated chloroform (1.6:1 v/v). Then 150 μL of a solution containing cyclohexanol (6 mg mL^{-1}) and chromium(III)acetylacetonate (3.6 mg mL^{-1}) was added, which served as an internal standard and relaxation reagent, respectively, and 75 μL of TMDP. NMR spectra were acquired without proton decoupling in CDCl_3 at 162 MHz, on a Bruker Ascend 400 MHz spectrometer. A total of 128 scans were acquired with a delay time of 6 s between two successive pulses. The spectra were processed using Topspin 3.1. All chemical shifts were reported in parts per million relative to the product of phosphorylated cyclohexanol (internal standard), which has been observed to give a doublet at 145.1 ppm. The content in hydroxyl groups (in mmol g^{-1}) was calculated on the basis of the integration of the phosphorylated cyclohexanol signal and by integration of the following spectral regions: aliphatic hydroxyls (150.8–146.4 ppm), condensed phenolic units (145.8–143.8 ppm; 142.2–140.2 ppm), syringyl phenolic hydroxyls (143.8–142.2 ppm), guaiacyl phenolic hydroxyls (140.2–138.2), *p*-hydroxyphenyl phenolic hydroxyls (138.2–137.0 ppm), and carboxylic acids (136.6–133.6 ppm).

4.3. Fractionation of the biorefinery lignins

The hydrolysis lignin (80 g dry-based, 80 g L^{-1}) was dissolved in acetone/water (3:1, V:V) for 12 h under magnetic stirring (c.a. 300 rpm). The soluble and the insoluble fractions were then separated via centrifugation (Eppendorf centrifuge 5804 R, Hamburg, Germany) for 20 min at 5000 rpm at 20 °C. The soluble fraction (also called lignin solution) was filtrated through glass microfiber filters GF/F by suction filtration to remove any traces of non-dissolved material. This fraction was stored in the solvent mixture until further use. The insoluble fraction (also called the lignocellulosic fraction) was dried in a fume hood for 2–3 days and manually ground to obtain a fine powder. The yield ratio after fractionation was 13:88 (w:w; dry basis) of the soluble fraction and the insoluble fraction respectively.

4.4. Preparation of lignocellulosic nanofibrils (LCNFs)

30 g (dry basis) of the acetone-insoluble residue of hydrolysis lignin was dispersed in 570 g of water (5 wt%) using an IKA T18 basic ULTRA-TURRAX device at speed 4 for 15 min. Fibrillation was performed by using a type M-110P microfluidizer (Microfluidics, Newton, Massachusetts, U.S.A.) in a single pass through a series of 400 and 200 μm chambers, followed by 12 passes through a series of 400 and 100 μm

chambers. The operating pressure was 2000 bar. The final concentration of the fiber dispersion was between 2.1 and 2.3 wt%.

4.5. Preparation of colloidal lignins particles (CLPs), cationic lignin and cationic CLPs (c-CLPs)

CLPs were prepared as reported previously [25] with a few modifications. The soda lignin was solubilized in an acetone:water mixture (3:1, V:V) at a concentration of ca. 11 g L^{-1} and stirred for 3 h, then filtrated through a Whatman® glass microfiber filter Grade GF/F to remove the insoluble parts. No solubilizations and filtrations were required for the SHL fraction, only a dilution in the same solvent mixture to reach a similar concentration. The lignin solution (either from the SHL fraction or the soda lignin) was, next, rapidly poured into water under vigorous magnetic stirring to obtain nanoprecipitation of spherical CLPs. The volume of water was three times higher than the lignin solution volume. The acetone was removed from the dispersion via dialysis (5–7 kDa membrane porosity) against deionized water. This procedure yielded an aqueous CLP dispersion with a concentration of ca. 2 g L^{-1} .

The cationic lignins were prepared as described previously [30] with a few modifications. A solution of SHL (containing 2 g of dry lignin) was concentrated until complete removal of acetone. Then the aqueous slurry of SHL (or dry SL) was solubilized in 0.2 M NaOH and heated at 70 °C. 8 g of glycidyltrimethylammonium (GTMAC) was added dropwise and the solution was stirred for 2 h at 70 °C. The reaction mixture was cooled down to room temperature with an ice bath. Finally, hydrochloric acid (37%) was added until pH 7 was reached. The product was dialysed (1 kDa membrane porosity) against deionized water to remove salt and the excess of GTMAC. The procedure yielded an aqueous cationic lignin solution with a concentration of ca. 4 g L^{-1} .

Both CLP dispersions and cationic lignin solutions were adjusted to pH 5 (using 0.1 M NaOH and 0.1 M HCl respectively) before fast adsorption of cationic lignins on CLPs under vigorous stirring.

4.6. Preparation of composite films

The composite films were prepared by pressure-assisted filtration [35]. CNF films were prepared by gently mixing CNFs (2.3 wt%, 1.8 g dry basis) with water to reach a concentration of 0.8 wt%. LCNF films were prepared by mixing CNFs (2.3 wt%, 0.27 g dry basis) and LCNFs (3.6 wt%, 1.5 g dry basis). Films containing CLP, cationic lignin or c-CLP films were prepared by mixing CNFs (2.3 wt%, 0.27 g dry basis), LCNFs (3.6 wt%, 1.5 g dry basis) and either CLPs, cationic lignin or c-CLPs (0.2 wt%, 0.2 g). For all samples, water was added to the pure CNFs prior to addition of the rest of the components, to have a final solid concentration of 0.8 wt%. The mixtures were filtrated through a 10 µm pore size open mesh Sefar Nitex polyamine monofilament fabric placed on the top of a VWR grade 415 filter paper. The wet films were dried between blotting papers either over a week under a 5 kg load at 23 °C and 50% relative humidity, or hot-pressed for 45 min at 1800 Pa load at 100 °C using a Carver Laboratory press (Fred S. Carver Inc.).

4.7. Atomic force microscopy

Dispersions of LCNFs were diluted in water in order to reach a concentration of 0.2 mg mL^{-1} . A minimum of 20 µL of each sample were spin-coated on mica plates at 2000 rpm during 2 min using a WS-650x-6NPP/Lite spin coater (Laurell Technologies Corporation, North Wales, USA). High-resolution AFM images were recorded with a MultiMode 8 AFM equipped with a NanoScope V controller (Bruker Corporation, Billerica, MA). The images were obtained in air in tapping mode using NCHV-A probes (Bruker) with a reported tip radius below 10 nm. Research NanoScope 8.15 software (Bruker) was used for image analysis, processing and correction (flattening was the only correction done).

4.8. Mechanical properties

The mechanical properties of the CNF (HP), LCNF (HP), CLP (HP) and LCNF (20%) nanocomposite films were analyzed by measuring the tensile stress and strain-at-break using a MTS 400/M tensile tester (MTS Systems Corporation), equipped with 200 N load cell. Rectangular strips of 50 mm in length and 5 mm in width were conditioned for 48 h at 50% RH at 23 °C and then glued onto paper frames to avoid slippage in the tensile clamps. Measurements were performed at a strain rate of 2 mm min^{-1} , in a controlled environment of 50% RH at 23 °C. At least six strips of each film were measured to obtain average values of tensile stress and strain-at-break.

4.9. Oxygen transmission rate

The oxygen transmission rate and permeability were tested according to ASTM D 3985–17 [94], using a Systech Illinois 8001 Oxygen Permeation analyzer (IL, USA). Due to the limited size of the samples, a mask (A Systech Illinois 8001 accessory) was used to decrease the surface area of the samples to 5 cm^2 . The pressure gradient was 1 atm, temperature was set to 23 °C and the relative humidity was set to 50% or 80%. Oxygen permeation was calculated from the OTR result using Eq. (1).

$$OP = OTR \cdot (l/\Delta P) \quad (1)$$

where l is the thickness of the samples and ΔP is the pressure gradient. The measurements at 50%RH were repeated twice while a single value was collected at 80% RH.

4.10. Antioxidant activity

The antioxidant assays were run using a method suitable for insoluble films [35], using tannic acid for calibration. Freshly prepared $\text{ABTS}^+ \cdot$ radical cation stock solution was diluted in water until reaching an absorbance of 0.6 at 734 nm at 25 °C before each series of measurements. Specimens of films (1–5 mg) were mixed with 2 mL of $\text{ABTS}^+ \cdot$ radical cation solution at 25 °C using a Stuart tube rotator SB2. For calibration, 20 µL aqueous tannic acid in the range of $0.02\text{--}0.50 \text{ mg mL}^{-1}$ was added into 2 mL of $\text{ABTS}^+ \cdot$ radical cation solution. The absorbance at 734 nm was measured at 25 °C exactly 1 h after mixing the components while protected from light. Reduction of the absorbance was calculated relatively to the blank ($\text{ABTS}^+ \cdot$ radical cation, 1 h after preparation). Films were analyzed in triplicates and standards in duplicates. Mean values were calculated and expressed as tannic acid equivalents (TAE) relative to the dry weight of the film sample, that is, mg of TAE g^{-1} of film. Prior to these assays, a kinetic study was completed with a circular specimen of film (CLP film) at different times (5, 15, 30 and 60 min) to determine the right amount of film to be used for the proper antioxidant activity evaluation.

4.11. Particle size and zeta potential

The particle size of CLPs and c-CLPs and the Zeta potential of CLPs, cationic lignin, c-CLPs and L-CNFs were measured using a Malvern Zetasizer Nano-ZS90 instrument (UK). The Zeta potential was determined with a dip cell probe and calculated from the electrophoretic mobility data using a Smoluchowski model. Three measurements for each sample were conducted to evaluate the reproducibility of the measurement. A volume of 1 mL was collected for all measurements with a concentration of 0.2 g L^{-1} .

4.12. Ecotoxicity

The two ecotoxicity tests were carried out according to OECD Test Guidelines: algal growth inhibition test (OECD 201) [95] and *Daphnia*

magna acute immobilization test (OECD 202) [96]. Two measurement methods were applied to determine the algal biomass in the OECD 201 test: cell count (Beckman Coulter Z2 Particle Counter) and in vivo fluorescence (Perkin Elmer Victor X3, excitation wavelength 436 nm / emission wavelength 680 nm). Aqueous dispersions of lignin nanoparticles (1.6 g L⁻¹ in deionized water) were diluted in the respective test media to achieve a concentration of 0.5 g L⁻¹. The concentration ranges for each ecotoxicity test were prepared from the aforementioned dispersion. Negative control samples containing only lignin nanoparticles at the same concentrations were analyzed in parallel to identify potential interferences of lignin suspension on algal cell fluorescence and cell counting.

4.13. Life cycle assessment

The LCA method follows the ISO 14040 [97] and ISO 14044 standard [98]. The functional unit is 1 kg of dry nanocomposite film production. The system boundary is cradle to gate. The allocation of multi-output of the fractionation process is based on mass. The impact assessment method is based on the global warming potentials (GWP) from the Intergovernmental Panel on Climate Change (IPCC) Fifth Assessment Report [99]. The primary data for building the life cycle inventory (LCI) data are collected from the experiment data in this study. Secondary data, such as electricity and solvent production are based on a dataset provided in the ecoinvent v3.5 database [100]. The CNF production data is based on Arvidsson et al. [83]. The detailed process data, LCI datasets and emission factors are available in Table S6 and Table S7. The modelling and calculation are performed with the SimaPro software version 9.1.

Declaration of Competing Interest

The authors declare that they have no known competing financial interests or personal relationships that could have appeared to influence the work reported in this paper.

Acknowledgements

This project has received funding from the Bio Based Industry Joint Undertaking under the European Union's Horizon 2020 research and innovation programme under grant agreement No 720303. We are grateful for the support by the FinnCERES Materials Bioeconomy Ecosystem and the work made use of Aalto University Bioeconomy Facilities. Joseph Campbell is thanked for proofreading the manuscript.

Author contribution

G.N.R. designed the experiments with M.F. M.H.-S. and M.Ö. F.P. and S.B. were responsible of lignin characterizations and provided the solubility data.

M.F. conducted the tensile experiments and assisted in the preparation of the composite films.

G.N.R. prepared the CLPs, the c-CLPs and the composite films. He also collected the AFM images, conducted the antioxidant assays and characterization of CLPs.

The ecotoxicity evaluation was performed by P.P., T.J. and G.M. H.K. determined the oxygen permeability of all the films.

G.N.R. wrote the manuscript with the contribution from all authors. All authors approved the final version of the manuscript.

Appendix A. Supplementary data

Supplementary data to this article can be found online at <https://doi.org/10.1016/j.susmat.2021.e00269>.

References

- [1] A. Chamas, H. Moon, J. Zheng, Y. Qiu, T. Tabassum, J.H. Jang, M. Abu-Omar, S.L. Scott, S. Suh, *ACS Sustain. Chem. Eng.* 8 (2020) 3494–3511.
- [2] A. Nag, A. Baksi, J. Ghosh, V. Kumar, S. Bag, B. Mondal, T. Ahuja, T. Pradeep, *ACS Sustain. Chem. Eng.* 7 (2019) 17554–17558.
- [3] Y. Chae, Y.-J. An, *Environ. Pollut.* 240 (2018) 387–395.
- [4] J.R. Jambeck, R. Geyer, C. Wilcox, T.R. Siegler, M. Perryman, A. Andrady, R. Narayan, *K.L. Law, Science* 347 (2015) 768–771.
- [5] M. Hoel, S. Kverndokk, *Resour. Energy Econ.* 18 (1996) 115–136.
- [6] R.J. Andres, J.S. Gregg, L. Losey, G. Marland, T.A. Boden, *Tellus Ser. B Chem. Phys. Meteorol.* 63 (2011) 309–327.
- [7] I. Malico, R. Nepomuceno Pereira, A.C. Gonçalves, A.M.O. Sousa, *Renew. Sust. Energ. Rev.* 112 (2019) 960–977.
- [8] S. Ross, D. Evans, *J. Clean. Prod.* 11 (2003) 561–571.
- [9] A. Soroudi, I. Jakubowicz, *Eur. Polym. J.* 49 (2013) 2839–2858.
- [10] P.T. Benavides, J.B. Dunn, J. Han, M. Biddy, J. Markham, *ACS Sustain. Chem. Eng.* 6 (2018) 9725–9733.
- [11] D. Bascovsky, M. Dallos, M. Worgetter, Status of 2nd Generation Biofuels Demonstration Facilities in June 2010, 2010.
- [12] A.J. Sannigrahi, Poulomi Ragauskas, J. Biobased Mater. Bioenergy 5 (2011) 514–519.
- [13] A.J. Ragauskas, G.T. Beckham, M.J. Biddy, R. Chandra, F. Chen, M.F. Davis, B.H. Davison, R.A. Dixon, P. Gilna, M. Keller, et al., *Science* 344 (2014) 1246843.
- [14] R. Wahlström, A. Kallioja, J. Heikkinen, H. Kyllönen, T. Tamminen, *Ind. Crop. Prod.* 104 (2017) 188–194.
- [15] X. Dong, M. Dong, Y. Lu, A. Turley, T. Jin, C. Wu, *Ind. Crop. Prod.* 34 (2011) 1629–1634.
- [16] Y. Zhang, W. Xu, X. Wang, S. Ni, E. Rosqvist, J.H. Smått, J. Pelttonen, Q. Hou, M. Qin, S. Willför, et al., *ACS Sustain. Chem. Eng.* 7 (2019) 6592–6600.
- [17] Y. Jiang, X. Liu, Q. Yang, X. Song, C. Qin, S. Wang, K. Li, *Cellulose* 26 (2019) 1577–1593.
- [18] Y. Chen, D. Fan, Y. Han, S. Lyu, Y. Lu, G. Li, F. Jiang, S. Wang, *Cellulose* 25 (2018) 6421–6431.
- [19] Ó. L. Ramos, R. N. Pereira, M. A. C. Cerequeira, J. R. Martins, J. A. Teixeira, F. X. Malcata, A. A. Vicente, *Handb. Food Bioeng.* (Eds.: A.M. Grumezescu and A.M. Holban), Academic Press, 2018, pp. 271–306.
- [20] A.H. Tayeb, M. Tajvidi, D. Bousfield, *Molecules* 25 (2020) 1344.
- [21] J. Sethi, M. Visanko, M. Österberg, J.A. Sirviö, *Carbohydr. Polym.* 203 (2019) 148–156.
- [22] I. Solala, M.C. Iglesias, M.S. Peresin, *Cellulose* 27 (2019) 1853–1877.
- [23] E. Rojo, M.S. Peresin, W.W. Sampson, I.C. Hoeger, J. Vartiainen, J. Laine, O.J. Rojas, *Green Chem.* 17 (2015) 1853–1866.
- [24] M. Österberg, M.H. Sipponen, B.D. Mattos, O.J. Rojas, *Green Chem.* 22 (2020) 2712–2733.
- [25] T. Zou, M.H. Sipponen, M. Österberg, *Front. Chem.* 7 (2019) 370.
- [26] P. Figueiredo, K. Lintinen, A. Kiriazis, V. Hynninen, Z. Liu, T. Bauleth-Ramos, A. Rahikallala, A. Correia, T. Kohout, B. Sarmento, et al., *Biomaterials* 121 (2017) 97–108.
- [27] M.-L. Mattinen, G. Riviere, A. Henn, R. Nugroho, T. Leskinen, O. Nivala, J. Valle-Delgado, M. Kostianinen, M. Österberg, *Nanomaterials* 8 (2018) 1001.
- [28] Y. Qian, X. Zhong, Y. Li, X. Qiu, *Ind. Crop. Prod.* 101 (2017) 54–60.
- [29] M.L. Mattinen, J.J. Valle-Delgado, T. Leskinen, T. Anttila, G. Riviere, M. Sipponen, A. Paananen, K. Lintinen, M. Kostianinen, M. Österberg, *Enzym. Microb. Technol.* 111 (2018) 48–56.
- [30] M.H. Sipponen, M. Smyth, T. Leskinen, L.S. Johansson, M. Österberg, *Green Chem.* 19 (2017) 5831–5840.
- [31] F. Kong, K. Parhiala, S. Wang, P. Fatehi, *Eur. Polym. J.* 67 (2015) 335–345.
- [32] G.N. Rivière, A. Korpi, M.H. Sipponen, M.A. Kostianinen, M. Österberg, *ACS Sustain. Chem. Eng.* 8 (2020) 4167–4177.
- [33] D. Tian, J. Hu, J. Bao, R.P. Chandra, J.N. Saddler, C. Lu, *Biotechnol. Biofuels* 10 (2017) 1–11.
- [34] W. Yang, F. Dominici, E. Fortunati, J.M. Kenny, D. Puglia, *Ind. Crop. Prod.* 77 (2015) 833–844.
- [35] M. Farooq, T. Zou, G. Riviere, M.H. Sipponen, M. Österberg, *Biomacromolecules* 20 (2019) 693–704.
- [36] O. Cusola, O.J. Rojas, M.B. Roncero, *ACS Appl. Mater. Interfaces* 11 (2019) 45226–45236.
- [37] X. Wang, S. Wang, W. Liu, S. Wang, L. Zhang, R. Sang, Q. Hou, J. Li, *Carbohydr. Polym.* 225 (2019) 115213.
- [38] W. Yang, J.S. Owczarek, E. Fortunati, M. Kozanecki, A. Mazzaglia, G.M. Balestra, J.M. Kenny, L. Torre, D. Puglia, *Ind. Crop. Prod.* 94 (2016) 800–811.
- [39] Z.H. Liu, N. Hao, S. Shinde, M.L. Olson, S. Bhagia, J.R. Dunlap, K.C. Kao, X. Kang, A.J. Ragauskas, J.S. Yuan, *ACS Sustain. Chem. Eng.* 7 (2019) 2634–2647.
- [40] S. Yildirim, B. Röcker, M.K. Pettersen, J. Nilsen-Nygaard, Z. Ayhan, R. Rutkaite, T. Radusin, P. Suminska, B. Marcos, V. Coma, *Compr. Rev. Food Sci. Food Saf.* 17 (2018) 165–199.
- [41] M. Lievonen, J.J. Valle-Delgado, M.-L. Mattinen, E.-L. Hult, K. Lintinen, M.A. Kostianinen, A. Paananen, G.R. Szilvay, H. Setälä, M. Österberg, *Green Chem.* 18 (2016) 1416–1422.
- [42] T. Leskinen, M. Smyth, Y. Xiao, K. Lintinen, M.-L. Mattinen, M.A. Kostianinen, P. Oinas, M. Österberg, *Nord. Pulp Pap. Res. J.* 32 (2017) 586–596.
- [43] Z.H. Liu, N. Hao, S. Shinde, Y. Pu, X. Kang, A.J. Ragauskas, J.S. Yuan, *Green Chem.* 21 (2019) 245–260.
- [44] M. Ma, L. Dai, J. Xu, Z. Liu, Y. Ni, *Green Chem.* (2020), <https://doi.org/10.1039/d0gc00377h>.

- [45] A.C. Rohr, S.L. Campleman, C.M. Long, M.K. Peterson, S. Weatherstone, W. Quick, A. Lewis, *Int. J. Environ. Res. Public Health* 12 (2015) 8542–8605.
- [46] D.J.F. Slatter, H. Sattar, C.H. Medina, G.E. Andrews, H.N. Phylaktou, B.M. Gibbs, *J. Loss Prev. Process Ind.* 36 (2015) 318–325.
- [47] J.P. Zhao, G.F. Tang, Y.C. Wang, Y. Han, *Heliyon* 6 (2020), e03457.
- [48] A. Santandrea, A. Vignes, A. Krietsch, D. Brunello, L. Perrin, A. Laurent, O. Dufaud, *Process. Saf. Environ. Prot.* 138 (2020) 279–291.
- [49] R. Fang, X. Cheng, X. Xu, *Bioresour. Technol.* 101 (2010) 7323–7329.
- [50] D. Xiao, W. Ding, J. Zhang, Y. Ge, Z. Wu, Z. Li, *Chem. Eng. J.* 358 (2019) 310–320.
- [51] Y. Zhang, S. Ni, X. Wang, W. Zhang, L. Lagerquist, M. Qin, S. Willför, C. Xu, P. Fatehi, *Chem. Eng. J.* 372 (2019) 82–91.
- [52] S. Imlimtham, A. Correia, P. Figueiredo, K. Lintinen, V. Balasubramanian, A.J. Airaksinen, M.A. Kostianen, H.A. Santos, M. Sarparanta, *J. Biomed. Mater. Res. - Part A* 108 (2020) 770–783.
- [53] C. Frangville, M. Rutkevicius, A.P. Richter, O.D. Velev, S.D. Stoyanov, V.N. Paunov, *ChemPhysChem* 13 (2012) 4235–4243.
- [54] G. Libralato, F. Avezzi, A. Volpi Ghirardini, J. Hazard, *Mater.* 194 (2011) 435–439.
- [55] K. Hund-Rinke, A. Baun, D. Cui, T.F. Fernandes, R. Handy, J.H. Kinross, J.M. Navas, W. Peijnenburg, K. Schlich, B.J. Shaw, et al., *Nanotoxicology* 10 (2016) 1442–1447.
- [56] OECD [Organisation for Economic Cooperation and Development], *OECD 2020, Guidance Document on Aquatic and Sediment Toxicological Testing of Nanomaterials*, 2020.
- [57] Y.N. Chang, M. Zhang, L. Xia, J. Zhang, G. Xing, *Materials* 5 (2012) 2850–2871.
- [58] C.F. Klingshirn, *ChemPhysChem* 8 (2007) 782–803.
- [59] Q. Zhang, K. Zhang, D. Xu, G. Yang, H. Huang, F. Nie, C. Liu, S. Yang, *Prog. Mater. Sci.* 60 (2014) 208–337.
- [60] Q.L. Shimabuku, F.S. Arakawa, M. Fernandes Silva, P. Ferri Coldebella, T. Ueda-Nakamura, M.R. Fagundes-Klen, R. Bergamasco, *Environ. Technol.* 38 (2017) 2058–2069.
- [61] Y. Wu, Y. Qian, H. Lou, D. Yang, X. Qiu, *ACS Sustain. Chem. Eng.* 7 (2019) 15966–15973.
- [62] Y. Qian, X. Qiu, S. Zhu, *Green Chem.* 17 (2015) 320–324.
- [63] I. Bilnova, A. Ivask, M. Heinlaan, M. Mortimer, A. Kahru, *Environ. Pollut.* 158 (2010) 41–47.
- [64] V. Aruoja, H.C. Dubourguier, K. Kasemets, A. Kahru, *Sci. Total Environ.* 407 (2009) 1461–1468.
- [65] M.S. Peresin, K. Kammiovirta, H. Heikkinen, L.S. Johansson, J. Vartiainen, H. Setälä, M. Österberg, T. Tammelin, *Carbohydr. Polym.* 174 (2017) 309–317.
- [66] S. Domenek, A. Louaifi, A. Guinauld, S. Baumberger, *J. Polym. Environ.* 21 (2013) 692–701.
- [67] A. Tripathi, A. Ferrer, S.A. Khan, O.J. Rojas, *ACS Sustain. Chem. Eng.* 5 (2017) 2483–2492.
- [68] D.M. de Carvalho, C. Moser, M.E. Lindström, O. Sevastyanova, *Ind. Crop. Prod.* 127 (2019) 203–211.
- [69] T.M. Tenhunen, M.S. Peresin, P.A. Penttilä, J. Pere, R. Serimaa, T. Tammelin, *React. Funct. Polym.* 85 (2014) 157–166.
- [70] M. Österberg, J. Vartiainen, J. Lucenius, U. Hippel, J. Seppälä, R. Serimaa, J. Laine, *ACS Appl. Mater. Interfaces* 5 (2013) 4640–4647.
- [71] U. Edlund, Y.Z. Ryberg, A.C. Albertsson, *Biomacromolecules* 11 (2010) 2532–2538.
- [72] A. Majira, B. Godon, L. Foulon, J.C. van der Putten, L. Cézard, M. Thierry, F. Pion, A. Bado-Nilles, P. Pandard, T. Jayabalan, et al., *ChemSusChem* 12 (2019) 4799–4809.
- [73] V. Ugartondo, M. Mitjans, M.P. Vinardell, *Bioresour. Technol.* 99 (2008) 6683–6687.
- [74] V. Ugartondo, M. Mitjans, M.P. Vinardell, *Ind. Crop. Prod.* 30 (2009) 184–187.
- [75] T. Dizhbite, G. Telysheva, V. Jurkane, U. Viesturs, *Bioresour. Technol.* 95 (2004) 309–317.
- [76] V. Aguié-Béghin, L. Foulon, P. Soto, D. Croinier, E. Corti, F. Legée, L. Cézard, B. Chabbert, M.N. Maillard, W.J.J. Huijgen, et al., *J. Agric. Food Chem.* 63 (2015) 10022–10031.
- [77] J. Chen, J. Yang, L. Ma, J. Li, N. Shahzad, C.K. Kim, *Sci. Rep.* 10 (2020) 1–9.
- [78] R.P. Bangalore Ashok, P. Oinas, K. Lintinen, G. Sarwar, M.A. Kostianen, M. Österberg, *Green Chem.* 20 (2018) 4911–4919.
- [79] D. Koch, M. Paul, S. Beisl, A. Friedl, B. Mihalyi, *J. Clean. Prod.* 245 (2020) 118760.
- [80] H. Sixta, in: H. Sixta (Ed.), *Handb. Pulp*, WILEY-VCH Verlag, Weinheim, Germany 2006, pp. 189–229.
- [81] GN Solids Control, Decanter centrifuge GNLW223D, can be found under https://www.gnsolidscontrol.com/decanting-centrifuge/?gclid=Cj0KCQjw0rt4BRCTARIsAB0_48PeAV96t8vPBmkJ-dNaDFVhkpGtHZeEOCeL61Z0eE7lp02JzeVAAAn-tEALw_wcB 2018 Accessed July 6, 2020.
- [82] Büchi, Rotavapor® R-220 Pro, can be found under <https://www.buchi.com/en/products/industrial-evaporation/rotavapor-r-220-pro> 2020 Accessed July 6, 2020.
- [83] R. Arvidsson, D. Nguyen, M. Svanström, *Environ. Sci. Technol.* 49 (2015) 6881–6890.
- [84] T. Tammelin, U. Hippel, A. Salminen, *Method for the Preparation of NFC Films on Supports*, 2018 WO2013060934 A3.
- [85] E. Fortunati, W. Yang, F. Luzzi, J. Kenny, L. Torre, D. Puglia, *Eur. Polym. J.* 80 (2016) 295–316.
- [86] R.P. Bangalore Ashok, Y. Xiao, K. Lintinen, P. Oinas, M.A. Kostianen, M. Österberg, *Colloids Surf. A Physicochem. Eng. Asp.* 587 (2020) 124228.
- [87] M. Tobiszewski, J. Namieśnik, F. Pena-Pereira, *Green Chem.* 19 (2017) 1034–1042.
- [88] M.H. Sipponen, H. Lange, C. Crestini, A. Henn, M. Österberg, *ChemSusChem* 12 (2019) 2039–2054.
- [89] A. Swerin, L. Odberg, T. Lindström, *Nord. Pulp Pap. Res. J.* 5 (2007) 188–196.
- [90] P. Eronen, J. Laine, J. Ruokolainen, M. Österberg, *J. Colloid Interface Sci.* 373 (2012) 84–93.
- [91] C.W. Dence, in: S.Y. Lin, C.W. Dence (Eds.), *Methods Lignin Chem.* Springer-Verlag, Berlin Heidelberg 1992, p. 33.
- [92] M.H. Sipponen, C. Lapiere, V. Méchin, S. Baumberger, *Bioresour. Technol.* 133 (2013) 522–528.
- [93] A. Granata, D.S. Argyropoulos, *J. Agric. Food Chem.* 43 (1995) 1538–1544.
- [94] ASTM2005.
- [95] OECD [Organisation for Economic Cooperation and Development], *OECD Guidelines for the Testing of Chemicals, Section 2 "Test No. 201: Freshwater Alga and Cyanobacteria, Growth Inhibition Test"*, Paris, 2011.
- [96] OECD [Organisation for Economic Cooperation and Development], *OECD Guidelines for the Testing of Chemicals, Section 2 "Test No. 202: Daphnia Sp. Acute Immobilisation Test"*, Paris, 2004.
- [97] ISO 14040: Environmental Management - Life Cycle Assessment - Principles and Framework2006.
- [98] ISO 14044: Environmental Management - Life Cycle Assessment - Requirements and Guidelines2006.
- [99] IPCC, *Climate Change 2014: Synthesis Report*, Geneva, Switzerland, 2014.
- [100]ecoinvent, *ecoinvent Version 3.5 2020*, can be found under <https://www.ecoinvent.org/database/database.html> 2020 Accessed July 6, 2020.